Electronic Supplementary Material (ESI) for RSC Advances.

Thermally Stable Mesoporous Tetragonal Zirconia Through Surfactant-Controlled Synthesis and Si-Stabilization

Ken Luca Abel [a)], *Sebastian Weber* [b),c)], *David Poppitz* [a)], *Juliane Titus* [a)], *Thomas L. Sheppard* [b),c)] *and Roger Gläser* [a)*]

[a)] Institute of Chemical Technology, Universität Leipzig, Linnéstr. 3, 04103 Leipzig, Germany

[b)] Institute for Chemical Technology and Polymer Chemistry, Karlsruhe Institute of Technology, Engesserstraße 20, 76131 Karlsruhe, Germany

[*] corresponding author (roger.glaeser@uni-leipzig.de)

Supporting Information

S1 Temperature Dependency of Crystal Structure and Textural Properties

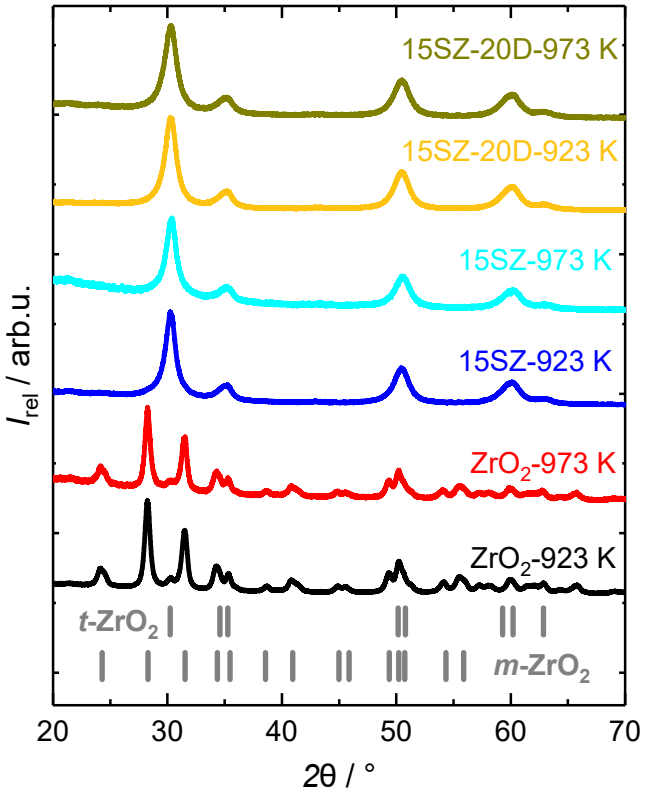

Fig. S1: XRD patterns of zirconia samples, calcined at either 923 K or 973 K.

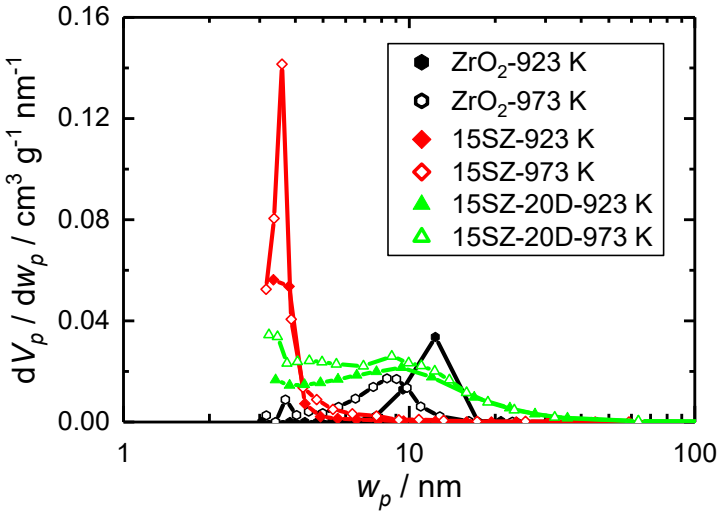

Fig. S2: BJH pore width distributions of zirconia samples, calcined at either 923 K or 973 K, determined via N_2 sorpion.

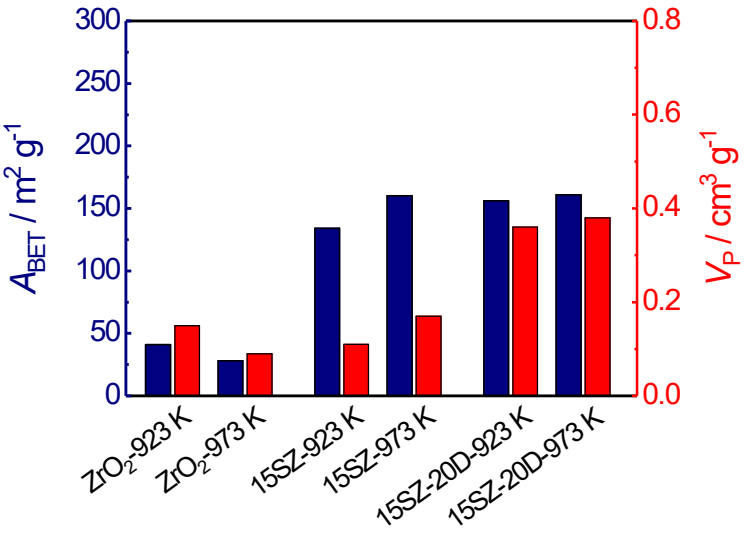

Fig. S3: Specific surface areas and pore volumes of zirconia samples, calcined at either 923 K or 973 K, determined via N_2 sorption.

S2 Exemplary N_2 Sorption Isotherms

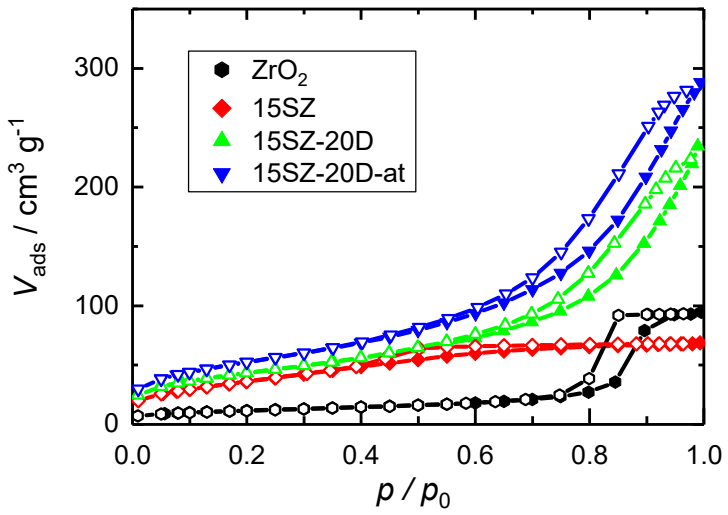

Fig. S4: N_2 sorption isotherms of zirconia samples calcined at 923 K; solid and open symbols represent the adsorption and desorption branch, respectively. Si mass fraction, DDA molar fraction and NH_4OH solution treatment are indicated with “15S”, “-20D” and “-at”, respectively.

S3 Stabilization of *t*-ZrO_2 by Si

S3.1 XRD and SAED patterns of pure ZrO_2 and sample 15SZ

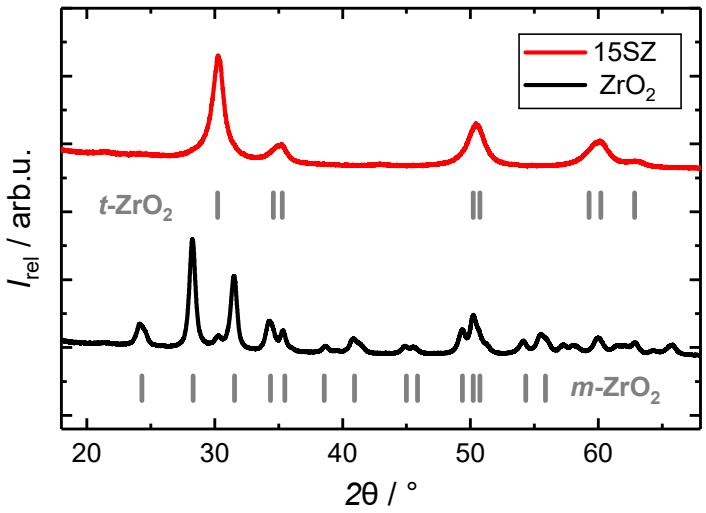

Fig. S5: XRD patterns of pure ZrO_2 and 15SZ calcined at 923 K.

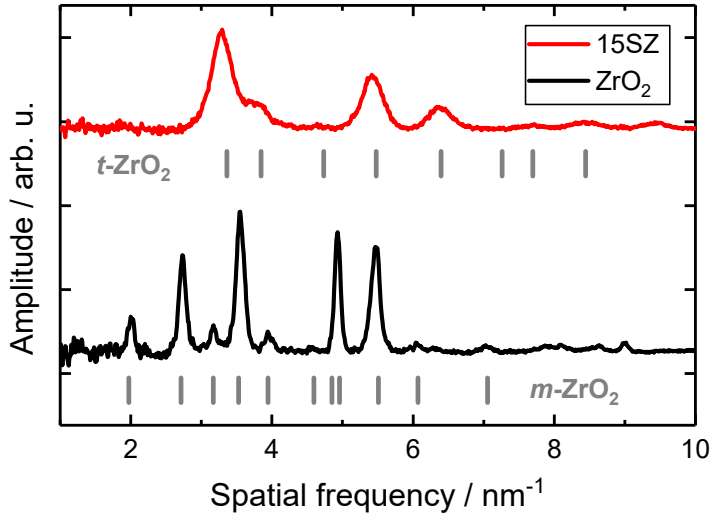

Fig. S6: Selected area electron diffraction (SAED) patterns of pure ZrO_2 and 15SZ, calcined at 923 K.

S3.2 Rietveld Refinements of pure ZrO_2 and SiO_2-ZrO_2 Samples

Topas software by Bruker [1] was used for Rietveld refinements of PXRD data [2,3]. An instrumental and emission profile was obtained for a LaB_6 standard to correct for peak broadening and influences on the measurement based on the instrument. Refinements were done using the fundamental parameters approach implemented in Topas [4,5]. Microstructure analysis was done using the double-Voigt approach by Balzar as implemented in Topas to describe the crystallite size and microstrain broadening by the sample [6]. Background correction was done with a 5^{th} order Chebychev polynomial. Initial structural models for monoclinic ZrO_2 by Smith *et al.* [7] and tetragonal ZrO_2 by Bondars *et al.* [8] were used for refinement. Refined diffraction patterns and obtained refined structural data are shown in Figures S1-S7 and Tables S1-S7. Thermal displacement parameters B_{iso} for both phases were not refined and were fixed to 0.48 and 0.3 for Zr and O, respectively as reported by Bondars *et al.* [8].

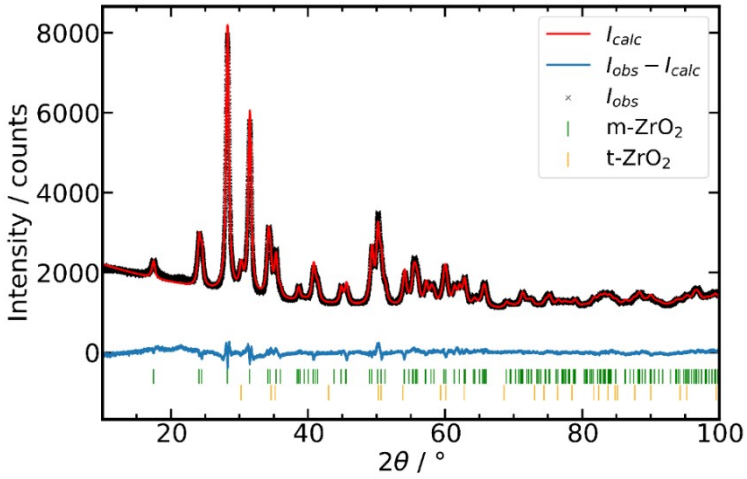

Fig. S7: Rietveld refinement of the pure ZrO_2 sample, calcined at 923 K; black crosses measured intensity, red line calculated intensity and blue line difference between measured and calculated intensity; green lines Bragg marker tetragonal ZrO_2; R_{exp} = 2.41, R_{wp} = 2.85, R_p = 2.22, GOF = 1.18.

Tab. S1: Structural data obtained from Rietveld refinement of the pure ZrO_2 sample, calcined at 923 K.

Phase		**ZrO_2 monoclinic**		**ZrO_2 tetragonal**	
Space group		$P2_1/c$ (No. 14)		$P4_2/nmc$ (No. 137)	
Cell Volume in Å^3		140.572(11)		67.17(3)	
Cell Mass in u		492.891		246.446	
Crystallite Size *D* in nm		16.05(16)		10.4(5)	
Microstrain ε_0		0.000740(19)		0.00001(16)	
Crystal Density in g/cm^3		5.8224(5)		6.093(3)	
Phase Amount in wt.-%		94.9(7)		5.1(7)	
Lattice Parameters					
a in Å		5.1473(2)		3.6024(6)	
c in Å		5.3138(2)		5.1758(16)	
β in °		99.1021(18)		90	
Phase		**ZrO_2 monoclinic**			
Atom	*x*	*y*	*z*	B_{iso}	*occ*
Zr1	0.27628(11)	0.03771(10)	0.21109(11)	0.48	1
O1	0.0769(6)	0.3311(6)	0.3576(5)	0.3	1
O2	0.4648(7)	0.7516(4)	0.4820(10)	0.3	1
Phase		**ZrO_2 tetragonal**			
Atom	*x*	*y*	*z*	B_{iso}	*occ*
Zr1	3/4	1/4	1/4	0.48	1
O1	1/4	1/4	0.45(4)	0.3	1

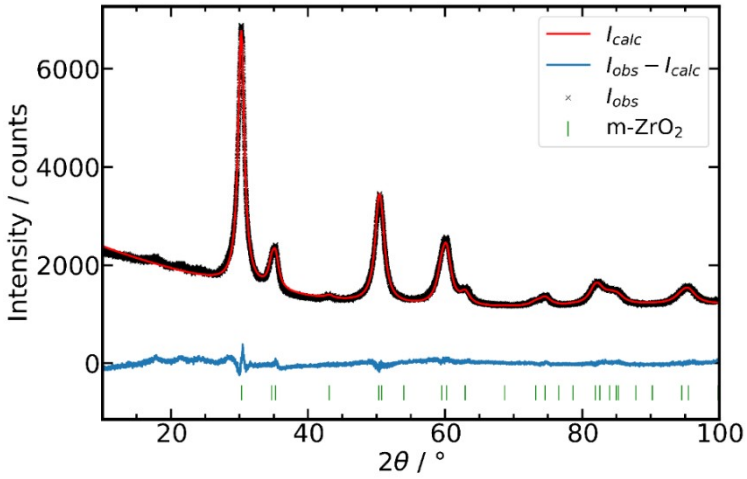

Fig. S8: Rietveld refinement of 15SZ calcined at 923 K; black crosses measured intensity, red line calculated intensity and blue line difference between measured and calculated intensity; green lines Bragg marker tetragonal ZrO_2; R_{exp} = 2.45, R_{wp} = 2.75, R_p = 2.27, GOF = 1.12.

Tab. S2: Structural data obtained from Rietveld refinement of 15SZ, calcined at 923 K.

Phase		**ZrO_2 tetragonal**			
Space group		$P4_2/nmc$ (No. 137)			
Cell Volume in Å^3		66.79(3)			
Cell Mass in u		246.446			
Crystallite Size *D* in nm		8.15(10)			
Microstrain ε_0		0.00300(5)			
Crystal Density in g/cm^3		6.127(3)			
Phase Amount in wt.-%		100			
Lattice Parameters					
a in Å		3.5960(7)			
c in Å		5.1649(12)			
β in °		90			
Phase		**ZrO_2 tetragonal**			
Atom	*x*	*y*	*z*	B_{iso}	*occ*
Zr1	3/4	1/4	1/4	0.48	1
O1	1/4	1/4	0.4544(5)	0.3	1

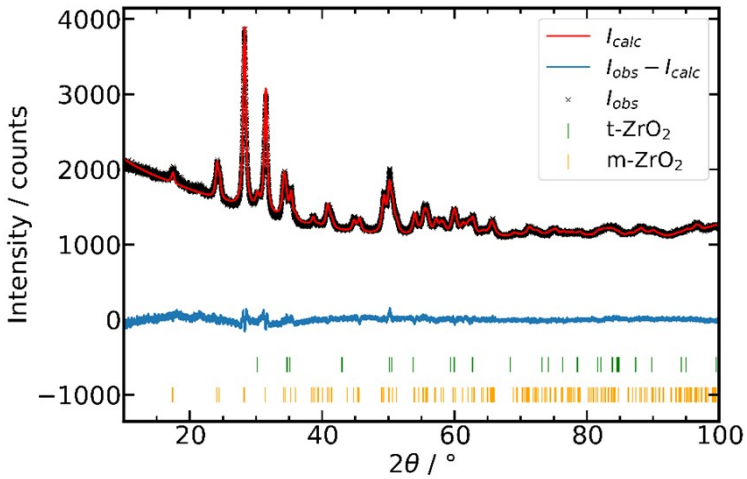

Fig. S9: Rietveld refinement of the pure ZrO_2 sample, calcined at 973 K; black crosses measured intensity, red line calculated intensity and blue line difference between measured and calculated intensity; green lines Bragg marker tetragonal ZrO_2; R_{exp} = 2.66, R_{wp} = 1.89, R_p = 1.47, GOF = 0.71.

Tab. S3: Structural data obtained from Rietveld refinement of the pure ZrO_2 sample, calcined at 973 K.

Phase		**ZrO_2 monoclinic**		**ZrO_2 tetragonal**	
Space group		*P*2$_1$/*c* (No. 14)		*P*4$_2$/*nmc* (No. 137)	
Cell Volume in Å^3		140.84(3)		67.43(8)	
Cell Mass		492.891		246.446	
Crystallite Size *D* in nm		23.7(6)		9.5(5)	
Microstrain ε_0		0.00168(5)		-	
Crystal Density in g/cm^3		5.8111(10)		6.069(7)	
Phase Amount in wt.-%		95.28(16)		4.72(16)	
Lattice Parameters					
a in Å		5.1527(5)		3.6122(15)	
c in Å		5.3157(5)		5.168(4)	
β in °		98.997(4)		90	
Phase		**ZrO_2 monoclinic**			
Atom	*x*	*y*	*z*	B_{iso}	*occ*
Zr1	0.2750(3)	0.0363(2)	0.2115(3)	0	1
O1	0.0697(15)	0.3290(13)	0.3574(12)	0	1
O2	0.4606(17)	0.7469(9)	0.477(2)	0	1
Phase		**ZrO_2 tetragonal**			
Atom	*x*	*y*	*z*	B_{iso}	*occ*
Zr1	3/4	1/4	1/4	0	1
O1	1/4	1/4	0.5(5)	0	1

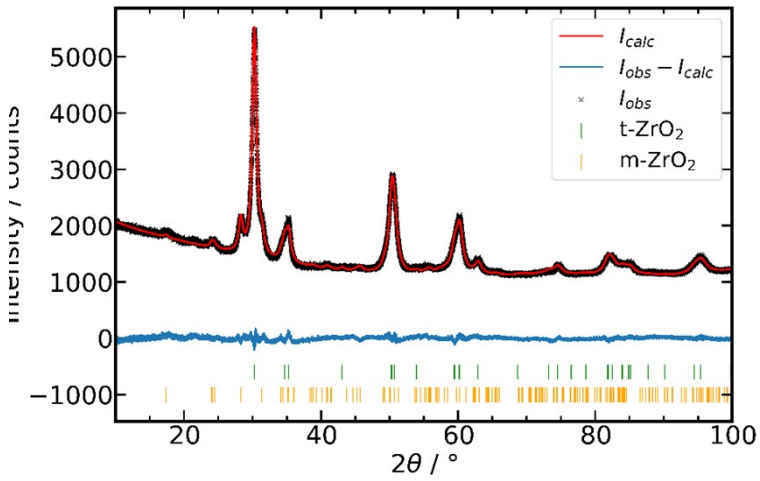

Fig. S10: Rietveld refinement of sample 5SZ, calcined at 973 K; black crosses measured intensity, red line calculated intensity and blue line difference between measured and calculated intensity; green lines Bragg marker tetragonal ZrO_2; R_{exp} = 2.61, R_{wp} = 1.88, R_p = 1.50, GOF = 0.72.

Tab. S4: Structural data obtained from Rietveld refinement of sample 5SZ, calcined at 973 K.

Phase		**ZrO_2 monoclinic**		**ZrO_2 tetragonal**	
Space group		$P2_1/c$ (No. 14)		$P4_2/nmc$ (No. 137)	
Cell Volume in Å^3		140.84(11)		66.925(11)	
Cell Mass		492.891		246.446	
Crystallite Size *D* in nm		17(2)		15.4(2)	
Microstrain ε_0		0.0031(3)		0.00241(4)	
Crystal Density in g/cm^3		5.811(4)		6.1148(10)	
Phase Amount in wt.-%		21.4(2)		78.6(2)	
Lattice Parameters					
a in Å		5.157(2)		3.5989(2)	
c in Å		5.310(2)		5.1671(5)	
β in °		98.64(2)		90	
Phase		**ZrO_2 monoclinic**			
Atom	*x*	*y*	*z*	B_{iso}	*occ*
Zr1	0.2155(11)	0.0294(12)	0.2179(14)	0	1
O1	0.054(6)	0.323(6)	0.381(6)	0	1
O2	0.524(9)	0.716(4)	0.497(16)	0	1
Phase		**ZrO_2 tetragonal**			
Atom	*x*	*y*	*z*	B_{iso}	*occ*
Zr1	3/4	1/4	1/4	0	1
O1	1/4	1/4	0.4536(9)	0	1

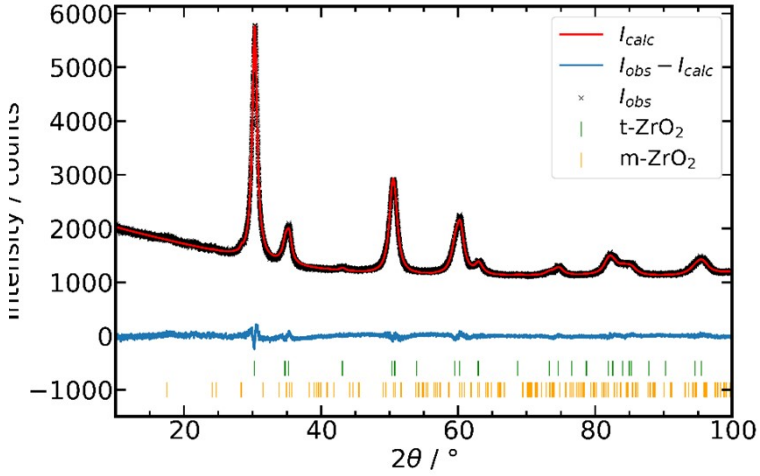

Fig. S11: Rietveld refinement of sample 8SZ, calcined at 973 K; black crosses measured intensity, red line calculated intensity and blue line difference between measured and calculated intensity; green lines Bragg marker tetragonal ZrO_2; R_{exp} = 2.61, R_{wp} = 1.77, R_p = 1.41, GOF = 0.68.

Tab. S5: Structural data obtained from Rietveld refinement of sample 8SZ, calcined at 973 K.

Phase		**ZrO_2 monoclinic**		**ZrO_2 tetragonal**	
Space group		$P2_1/c$ (No. 14)		$P4_2/nmc$ (No. 137)	
Cell Volume in Å^3		139.3(3)		66.754(12)	
Cell Mass		492.891		246.446	
Crystallite Size *D* in nm		21(5)		13.9(2)	
Microstrain ε_0		0.0031(3)		0.00314(4)	
Crystal Density in g/cm^3		5.875(14)		6.1305(11)	
Phase Amount in wt.-%		1.16(15)		98.84(15)	
Lattice Parameters					
a in Å		5.132(7)		3.5959(2)	
c in Å		5.356(7)		5.1625(6)	
β in °		98.94(9)		90	
Phase		**ZrO_2 monoclinic**			
Atom	*x*	*y*	*z*	B_{iso}	*occ*
Zr1	0.27580	0.04110	0.20820	0	1
O1	0.07030	0.33590	0.34060	0	1
O2	0.44230	0.75490	0.47890	0	1
Phase		**ZrO_2 tetragonal**			
Atom	*x*	*y*	*z*	B_{iso}	*occ*
Zr1	3/4	1/4	1/4	0	1
O1	1/4	1/4	0.4527(6)	0	1

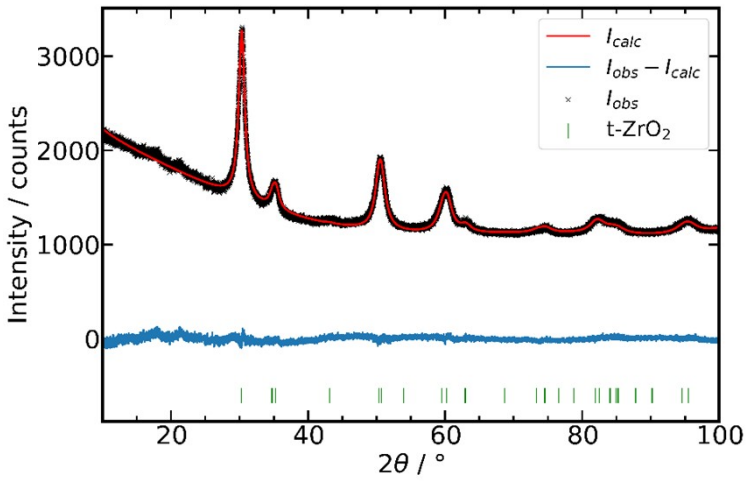

Fig. S12: Rietveld refinement of sample 15SZ, calcined at 973 K; black crosses measured intensity, red line calculated intensity and blue line difference between measured and calculated intensity; green lines Bragg marker tetragonal ZrO_2; R_{exp} = 2.66, R_{wp} = 1.71, R_p = 1.38, GOF = 0.64.

Tab. S6: Structural data obtained from Rietveld refinement of sample 15SZ, calcined at 973 K.

Phase		**ZrO_2 tetragonal**			
Space group		*$P4_2/nmc$* (No. 137)			
Cell Volume in Å^3		66.79(4)			
Cell Mass		246.446			
Crystallite Size *D* in nm		13.4(5)			
Microstrain ε_0		0.00468(11)			
Crystal Density in g/cm^3		6.128(3)			
Phase Amount in wt.-%		100			
Lattice Parameters					
a in Å		3.5979(7)			
c in Å		5.1592(19)			
Phase		**ZrO_2 tetragonal**			
Atom	*x*	*y*	*z*	B_{iso}	*occ*
Zr1	3/4	1/4	1/4	0.0	1
O1	1/4	1/4	0.470(2)	0.0	1

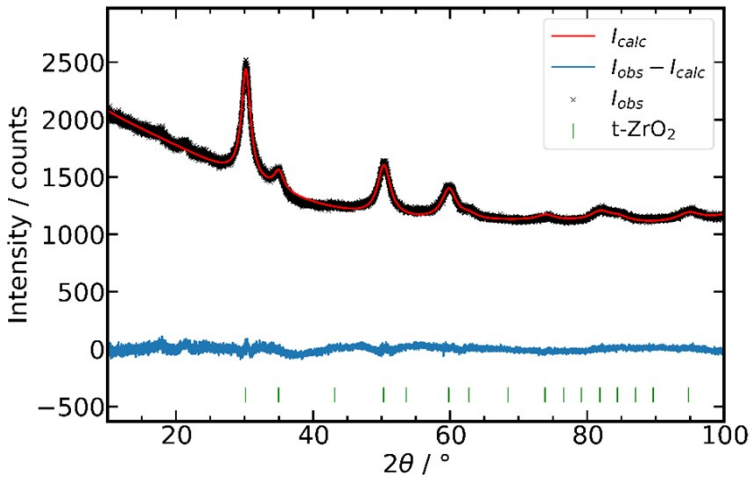

Fig. S13: Rietveld refinement of 19SZ, calcined at 973 K; black crosses measured intensity, red line calculated intensity and blue line difference between measured and calculated intensity; green lines Bragg marker tetragonal ZrO_2; R_{exp} = 2.69, R_{wp} = 1.63, R_p = 1.30, GOF = 0.61.

Tab. S7: Structural data obtained from Rietveld refinement of sample 19SZ, calcined at 973 K.

Phase		**ZrO_2 tetragonal**			
Space group		*$P4_2/nmc$* (No. 137)			
Cell Volume in Å^3		67.4(15)			
Cell Mass		246.446			
Crystallite Size *D* in nm		7.5(3)			
Microstrain ε_0		0.0064(2)			
Crystal Density in g/cm^3		6.07(14)			
Phase Amount in wt.-%		100			
Lattice Parameters					
a in Å		3.62(3)			
c in Å		5.13(8)			
Phase		**ZrO_2 tetragonal**			
Atom	*x*	*y*	*z*	B_{iso}	*occ*
Zr1	3/4	1/4	1/4	0.0	1
O1	1/4	1/4	0.50(3)	0.0	1

S4 Mesopore Generation in the Presence of Dodecylamine

S4.1 Electron Tomography Experiments

S4.1.1 Data collection and processing

The tilt series of high-angle annular dark field STEM images were collected with the Xplore3D software (FEI) over a tilt range of ±60°, with an increment of 2°. Alignment and reconstruction of the tilt series was performed using the TomoJ software plug-in for Fiji [9,10]. For alignment, translation correction by cross-correlation function followed by 3D landmarks alignment as implemented in the software was used [11]. The aligned projection series was then reconstructed by the simultaneous iterative reconstruction technique (SIRT) [12] and following discrete algebraic reconstruction technique (DART) [13]. The resultant reconstructed tomograms had a final voxel size of 0.64 nm. Image processing and analysis of the obtained tomograms was carried out using Avizo 9.7.0 (Thermo Fischer Scientific).

The lamellas prepared via focused ion beam (FIB) milling were mounted with a micromanipulator to a four-finger lift-out grid by Pt-gluing and further thinned to a thickness of about 200 nm in the region of interest for ET. The prepared lamellas are shown in Fig. S14 and Fig. S18. Overview HAADF-STEM images of the two samples are shown Fig. S15 and Fig. S19. The effective resolution d_{eff} of the reconstructed tomograms is estimated with the Crowther criterion [14]

$$d_{eff} = \pi * \frac{D}{m} \qquad (1)$$

with D as the particle diameter and m as the number of projections. For the tomograms we acquired each 60 projections and for D we estimate a value of 250 nm, slightly larger than the thickness of the lamellas. Based on these assumptions, the effective resolution of the reconstructed tomograms is estimated as 13 nm, while the voxel size is 0.64 nm.

Image processing and analysis of the reconstructed tomograms in Avizo 9.7.0 (Thermo Fischer) was done according the following described procedure. First the object was masked using the segmentation editor with the “Brush” and “Interpolation” tools to be able to separate pores from the background. For the masked object material and pores were labelled by thresholding. On each label an “Opening” operation was performed to remove small point artefacts. The material and pore labels were analyzed by ”Label Analysis” to determine the label volumes. Furthermore, on the pore label the ”Separate Objects” module was used to obtain separated pores for individual pore analysis. An

”Opening” module was used to remove point artefacts of the pore separation. The separated pores were then analyzed by ”Label Analysis” to determine characteristics of the individual pores, focusing on the pore volume and equivalent pore diameter d_{eq}, which is defined as following

$$d_{eq} = \sqrt[3]{\frac{6 * V_{3D}}{\pi}} \quad (2)$$

with V_{3D} as the voxel based calculated 3D volume of a single pore. In Fig. S16 and Fig. S20 the volume rendering of the material with the finally separated individual pores are shown for the two samples. The results of the “Label Analysis” were further analyzed to retrieve the porosity distribution depending on the equivalent pore diameter as shown in Fig. S17 and Fig. S21. For this purpose, the porosity of an individual pore is defined as ϕ_{ind}

$$\phi_{ind} = \frac{V_{P,ind}}{V_{p,tot} + V_{s,tot}} \quad (3)$$

With the individual pore volume $V_{P,\mathrm{ind}}$, the total pore volume $V_{P,tot}$ and the total solid material volume $V_{\mathrm{s,tot}}$.

The obtained distribution was then analyzed regarding its weighted numerical mean pore diameter and by fitting a Gaussian function. The difference of the mean values from the weighted numerical analysis and the fit is assumed as the standard deviation of the mean pore diameter from the numerical analysis. The results of the quantitative analysis of the tomograms for both samples are summarized in Tab. S8.

S4.1.2 Analysis of the pure ZrO_2 sample

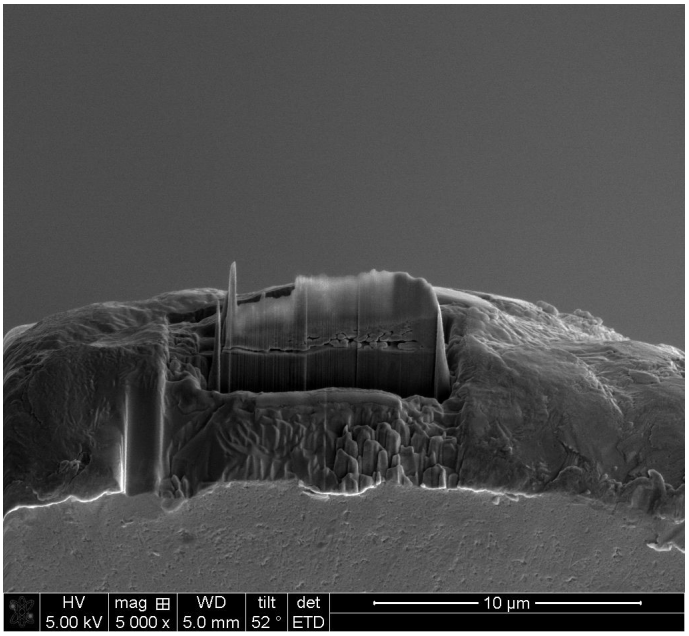

Fig. S14: SEM image of the lamella of the pure ZrO_2 sample calcined at 923 K, prepared via FIB attached to the lift-out grid for the ET measurement.

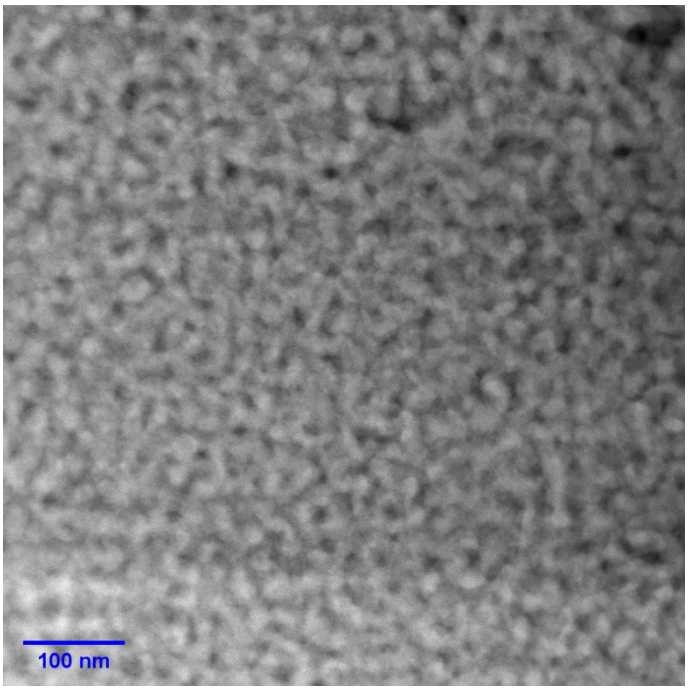

Fig. S15: Overview-HAADF-STEM image of the pure ZrO_2 sample, calcined at 923 K.

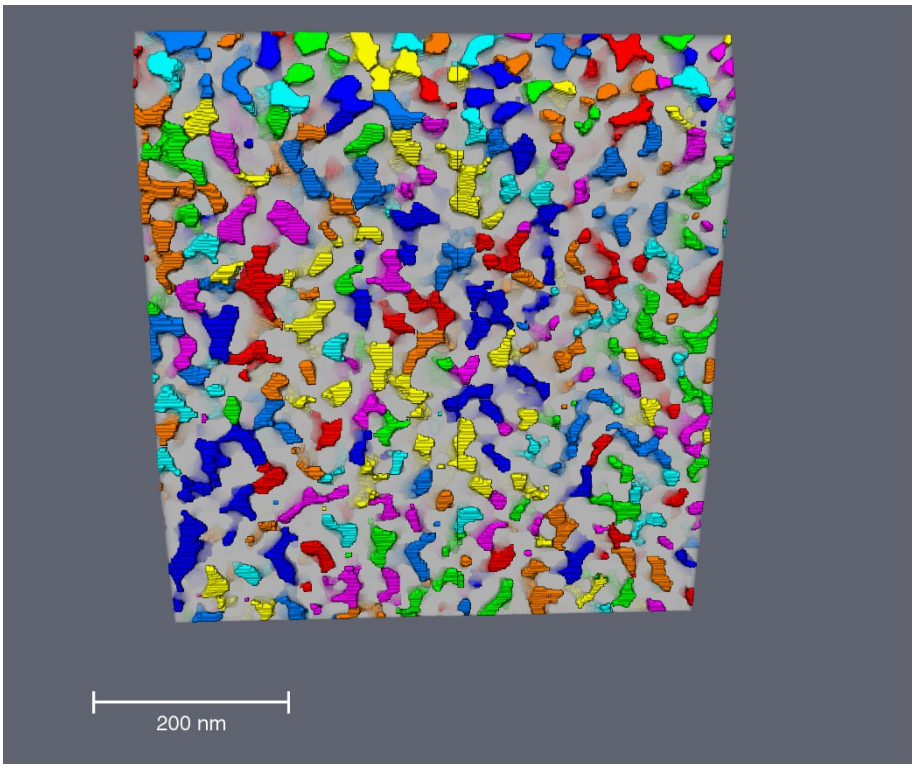

Fig. S16: Rendered volume of the 8-bit color labelled separated pores and the material (light grey) for the ET of the pure ZrO_2 sample calcined at 923 K.

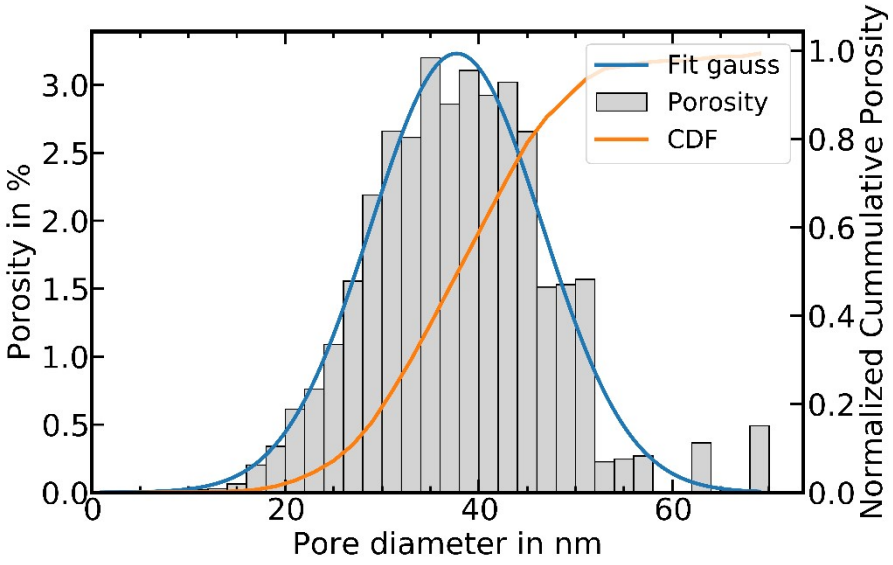

Fig. S17: Porosity distribution depending on the equivalent pore diameter based on image analysis of the ET of the pure ZrO_2 sample calcined at 923 K, with the fitted Gaussian (blue) and the cumulative distribution function (CDF, orange).

S4.1.3 Analysis of sample 15SZ-20D

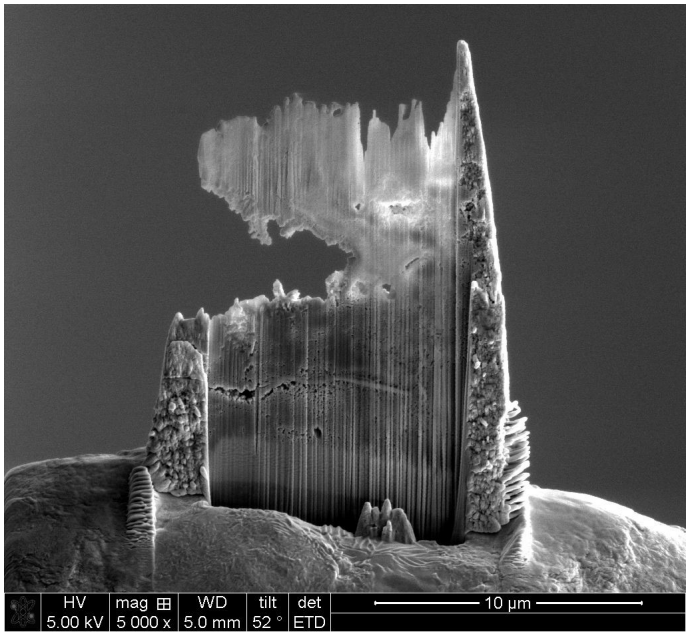

Fig. S18: SEM image of the lamella of sample 15SZ-20D, calcined at 923, prepared via FIB attached to the lift-out grid for the ET measurement.

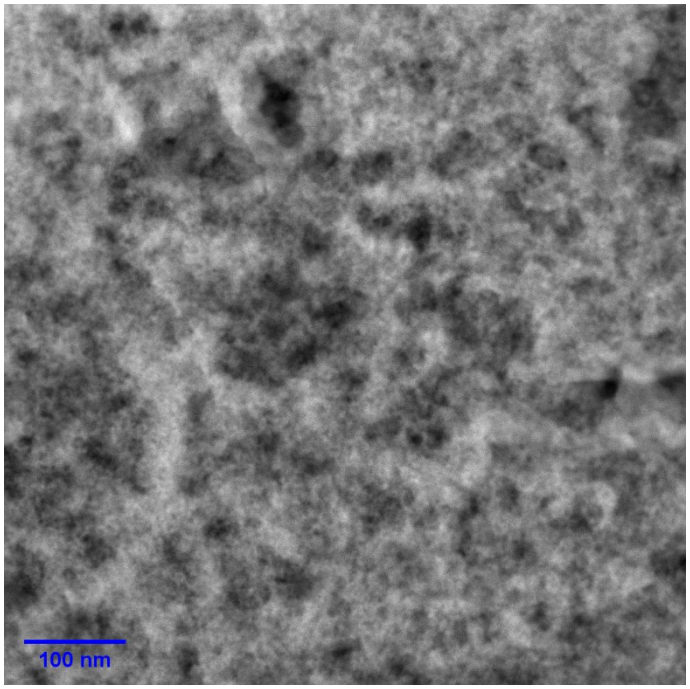

Fig. S19: Overview HAADF-STEM image of sample 15SZ-20D, calcined at 923 K.

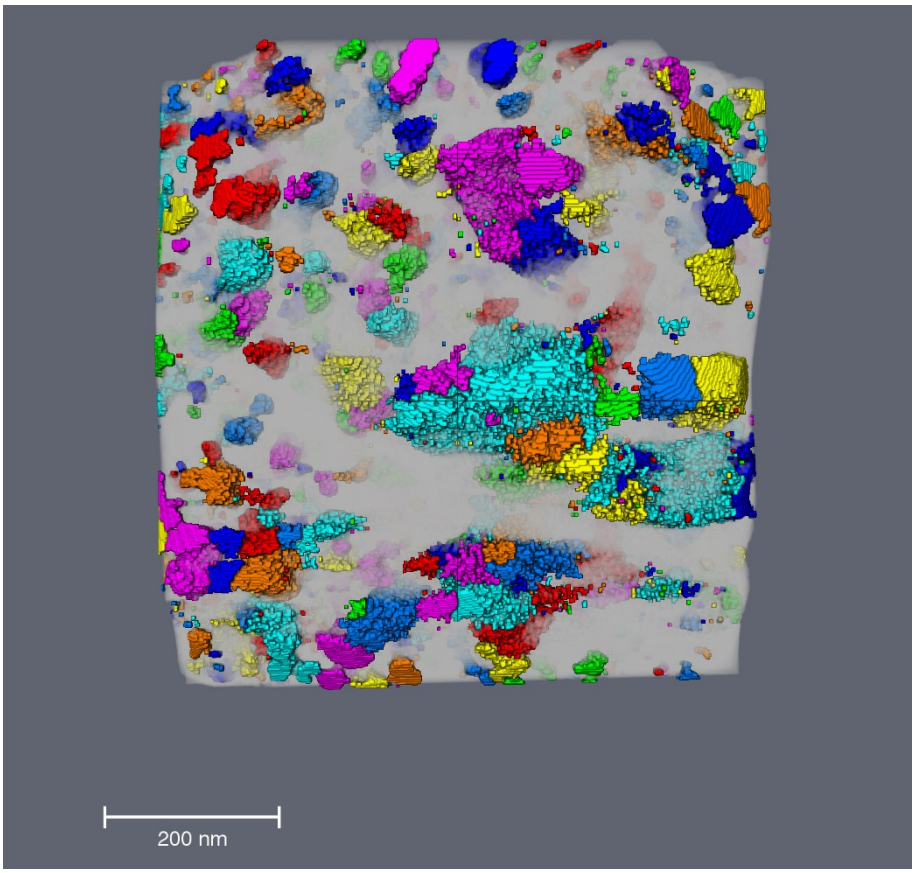

Fig. S20: Rendered volume of the 8-bit color labelled separated pores and the material (greyish) for the ET of sample 15SZ-20D, calcined at 923 K.

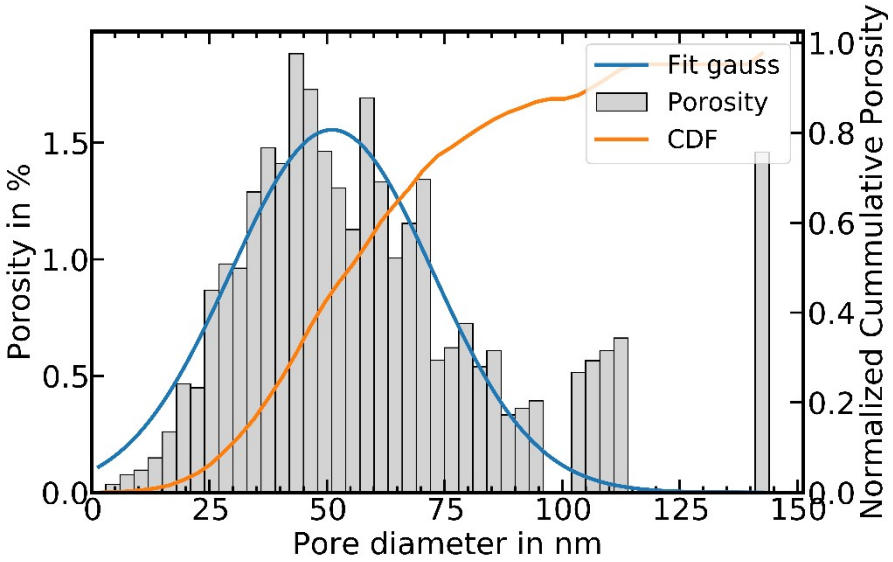

Fig. S21: Porosity distribution depending on the equivalent pore diameter based on image analysis of the ET of sample 15SZ-20D calcined at 923 K, with the fitted Gaussian (blue) and the cumulative distribution function (CDF, orange).

S4.1.4 Results from quantitative analysis of the ET

Tab. S8: Material volume, area and pore system information obtained from quantitative label analysis of the ET of samples pure ZrO_2 and 15SZ-20D, calcined at 923 K. Volume and area values are the sum of all individual pore and material labels. The mean equivalent pore diameter d_{eq} was calculated numerically from the distribution and via fitting a Gaussian to the distribution. The standard deviation of the numerical d_{eq} is assumed as the difference between the Gaussian fit and the numerical result.

Sample	***Z***	***15SZ-20D***
Volume Material $V_{s,tot}$ / nm^3	22397068.3	76084024.0
Area Material $A_{s,tot}$ / nm^2	3718566.7	9406104.5
Total Pore Volume $V_{P,tot}$ / nm^3	13312500.4	34546110.9
Total Pore Area $A_{P,tot}$ / nm^2	3283322.3	7138800.3
Total Porosity ϕ_{tot} / %	37.3	31.2
d_{eq} (Numerical) / nm	38.1 ± 0.4	60.8 ± 9.7
d_{eq} (Gaussian) / nm	37.7	51.1
R^2 Gaussian Fit	0.97	0.73

S4.2 Hg Porosimetry of the Sample 15SZ-20D

Hg Porosimetry analysis was conducted on a ThermoScientific PASCAL 140 (lower pressures) and a ThermoScientific PASCAL 440 (higher pressures). The contact angle used was 140° with a surface tension of 0.48 N m^{-1}.

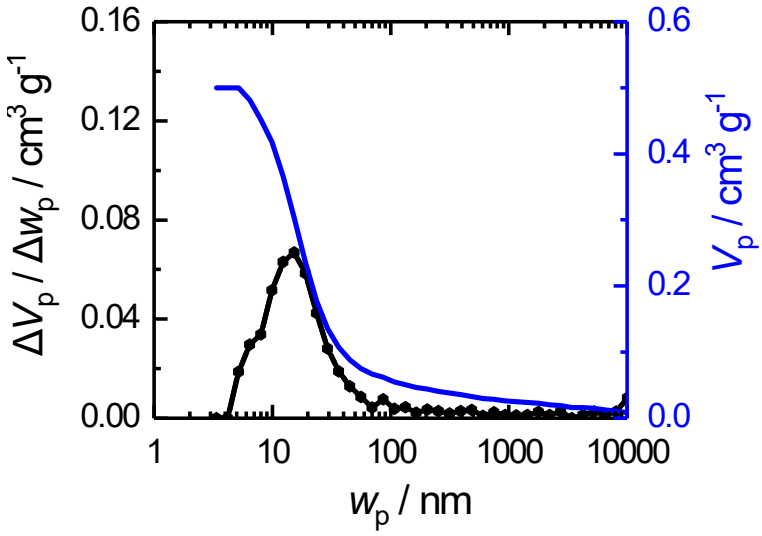

Fig. S22: Incremental (black line) and cumulative (blue line) specific pore volume of the sample 15SZ-20D calcined at 923 K, determined via Hg porosimetry.

S4.3 Rietveld Refinements of Zirconia Samples Prepared in Presence of DDA

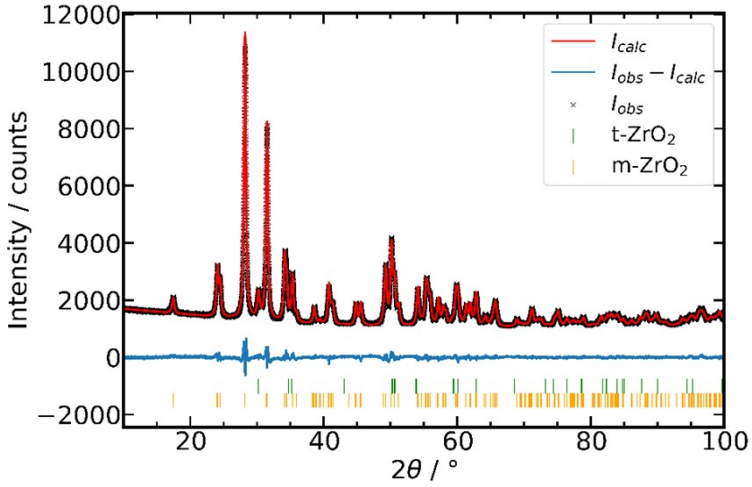

Fig. S23: Rietveld refinement of the sample Z-20D, calcined at 973 K ; black crosses measured intensity, red line calculated intensity and blue line difference between measured and calculated intensity; green lines Bragg marker tetragonal ZrO_2; R_{exp} = 2.51, R_{wp} = 2.31, R_p = 1.73, GOF = 0.92.

Tab. S9: Structural data obtained from Rietveld refinement of Z-20D, calcined at 973 K.

Phase		**ZrO_2 monoclinic**		**ZrO_2 tetragonal**	
Space group		P21/c (No. 14)		*$P4_2/nmc$* (No. 137)	
Cell Volume in Å^3		141.053(4)		67.337(12)	
Cell Mass in u		492.891		246.446	
Crystallite Size *D* in nm		25.03(12)		15.9(2)	
Microstrain ε_0		0.000466(7)		-	
Crystal Density in g/cm^3		5.80253(15)		6.0774(11)	
Phase Amount in wt.-%		95.02(4)		4.98(4)	
Lattice Parameters					
a in Å		5.15155(8)		3.6005(2)	
c in Å		5.32116(8)		5.1945(6)	
β in °		99.2052(8)		90	
Phase		**ZrO_2 monoclinic**			
Atom	*x*	*y*	*z*	B_{iso}	*occ*
Zr1	0.27541(6)	0.03950(6)	0.20965(6)	0	1
O1	0.0716(4)	0.3299(4)	0.3512(3)	0	1
O2	0.4523(4)	0.7539(3)	0.4749(5)	0	1
Phase		**ZrO_2 tetragonal**			
Atom	*x*	*y*	*z*	B_{iso}	*occ*
Zr1	3/4	1/4	1/4	0	1
O1	1/4	1/4	0.432(3)	0	1

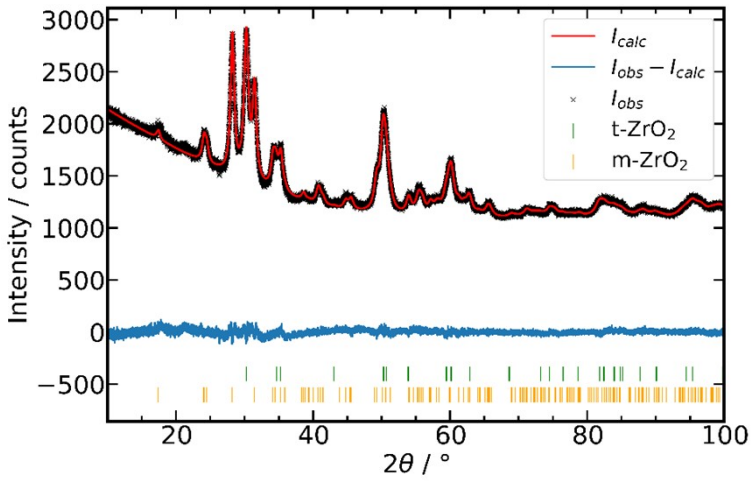

Fig. S24: Rietveld refinement of 5SZ-20D, calcined at 973 K; black crosses measured intensity, red line calculated intensity and blue line difference between measured and calculated intensity; green lines Bragg marker tetragonal ZrO_2; R_{exp} = 2.64, R_{wp} = 1.56, R_p = 1.23, GOF = 0.59.

Tab. S10: Structural data obtained from Rietveld refinement of 5SZ-20D, calcined at 973 K.

Phase		**ZrO_2 monoclinic**		**ZrO_2 tetragonal**	
Space group		$P2_1/c$ (No. 14)		$P4_2/nmc$ (No. 137)	
Cell Volume in Å^3		141.09(2)		67.134(12)	
Cell Mass		492.891		246.446	
Crystallite Size *D* in nm		14.6(2)		11.17(18)	
Microstrain ε_0		0.00171(5)		0.00176(6)	
Crystal Density in g/cm^3		5.8009(10)		6.0957(11)	
Phase Amount in wt.-%		61.92(11)		38.08(11)	
Lattice Parameters					
a in Å		5.1560(5)		3.6009(2)	
c in Å		5.3233(5)		5.1775(6)	
β in °		99.052(4)		90	
Phase		**ZrO_2 monoclinic**			
Atom	*x*	*y*	*z*	B_{iso}	*occ*
Zr1	0.2760(2)	0.0386(2)	0.2136(3)	0	1
O1	0.0742(14)	0.3337(12)	0.3671(11)	0	1
O2	0.4580(15)	0.7467(8)	0.4784(19)	0	1
Phase		**ZrO_2 tetragonal**			
Atom	*x*	*y*	*z*	B_{iso}	*occ*
Zr1	3/4	1/4	1/4	0	1
O1	1/4	1/4	0.4604(14)	0	1

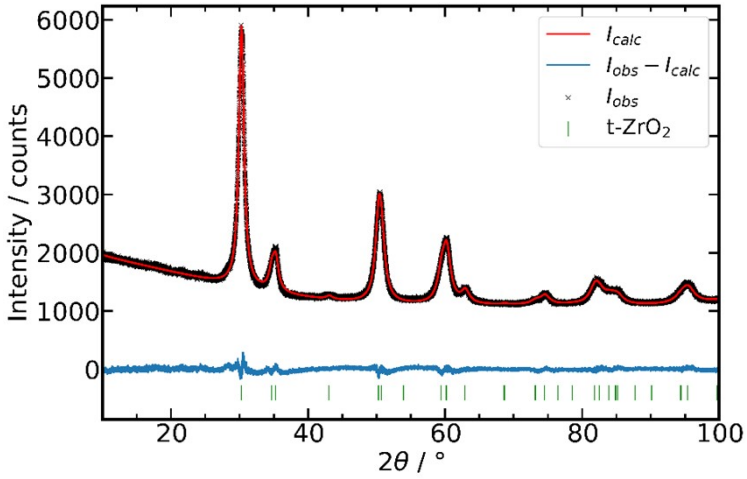

Fig. S25: Rietveld refinement of sample 10SZ-20D, calcined at 973 K; black crosses measured intensity, red line calculated intensity and blue line difference between measured and calculated intensity; green lines Bragg marker tetragonal ZrO_2; R_{exp} = 2.61, R_{wp} = 1.77, R_p = 1.41, GOF = 0.68.

Tab. S11: Structural data obtained from Rietveld refinement of sample 10SZ-20D, calcined at 973 K.

Phase		**ZrO_2 tetragonal**			
Space group		*$P4_2/nmc$* (No. 137)			
Cell Volume in Å^3		66.982(12)			
Cell Mass		246.446			
Crystallite Size *D* in nm		11.87(14)			
Microstrain ε_0		0.00301(4)			
Crystal Density in g/cm^3		6.1096(11)			
Phase Amount in wt.-%		100			
Lattice Parameters					
a in Å		3.5992(2)			
c in Å		5.1706(6)			
Phase		**ZrO_2 tetragonal**			
Atom	*x*	*y*	*z*	B_{iso}	*occ*
Zr1	3/4	1/4	1/4	0.0	1
O1	1/4	1/4	0.4522(6)	0.0	1

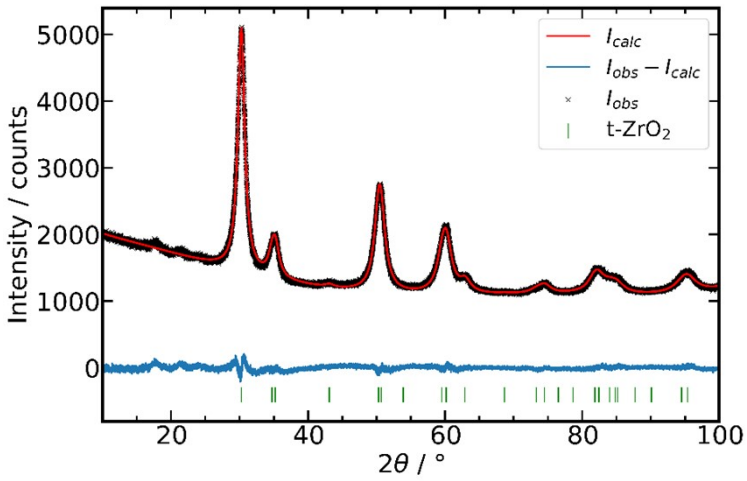

Fig. S26: Rietveld refinement of sample 15SZ-20D, calcined at 973 K; black crosses measured intensity, red line calculated intensity and blue line difference between measured and calculated intensity; green lines Bragg marker tetragonal ZrO_2; R_{exp} = 2.58, R_{wp} = 1.87, R_p = 1.48, GOF = 0.72.

Tab. S12: Structural data obtained from Rietveld refinement of sample 15SZ-20D, calcined at 973 K.

Phase		**ZrO_2 tetragonal**			
Space group		*$P4_2/nmc$* (No. 137)			
Cell Volume in Å^3		66.95(2)			
Cell Mass		246.446			
Crystallite Size *D* in nm		8.64(10)			
Microstrain ε_0		0.00399(5)			
Crystal Density in g/cm^3		6.1129(18)			
Phase Amount in wt.-%		100			
Lattice Parameters					
a in Å		3.6010(4)			
c in Å		5.1627(10)			
Phase		**ZrO_2 tetragonal**			
Atom	*x*	*y*	*z*	B_{iso}	*occ*
Zr1	3/4	1/4	1/4	0.0	1
O1	1/4	1/4	0.4547(7)	0.0	1

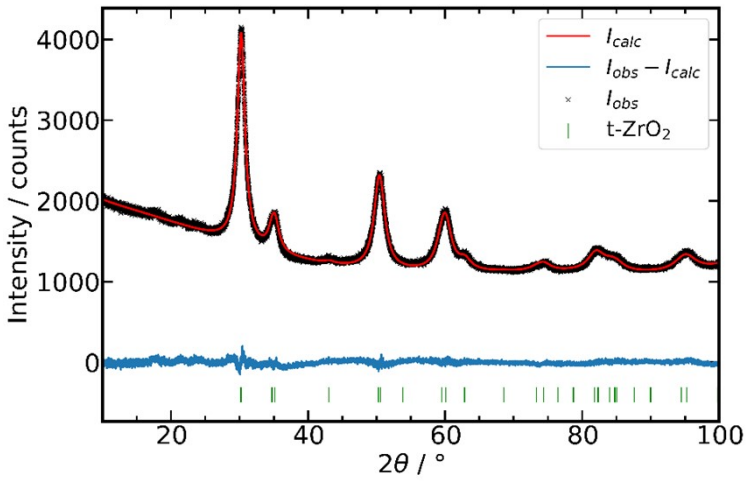

Fig. S27: Rietveld refinement of sample 29SZ-20D, calcined at 973 K; black crosses measured intensity, red line calculated intensity and blue line difference between measured and calculated intensity; green lines Bragg marker tetragonal ZrO_2; R_{exp} = 2.61, R_{wp} = 1.34, R_p = 1.34, GOF = 0.64.

Tab. S13: Structural data obtained from Rietveld refinement of sample 29SZ-20D, calcined at 973 K.

Phase		**ZrO_2 tetragonal**			
Space group		$P4_2/nmc$ (No. 137)			
Cell Volume in Å^3		67.09(3)			
Cell Mass		246.446			
Crystallite Size *D* in nm		8.10(12)			
Microstrain ε_0		0.00468(8)			
Crystal Density in g/cm^3		6.100(3)			
Phase Amount in wt.-%		100			
Lattice Parameters					
a in Å		3.6053(6)			
c in Å		5.1612(18)			
Phase		**ZrO_2 tetragonal**			
Atom	*x*	*y*	*z*	B_{iso}	*occ*
Zr1	3/4	1/4	1/4	0.0	1
O1	1/4	1/4	0.4560(9)	0.0	1

S4.4 Variation of the Surfactant during Zirconia Gelation

The synthesis of these samples was conducted according to the procedure reported in the main publication, with dodecylamine being replaced with hexadecylamine (Merck, 92 %), cetyltrimethylammoniumbromide (VWR, 99 %), palmitic acid (Aldrich, 99 %) or polyethylene glycol 20k (Merck, 99 %). A molar fraction of 20 mol-%, based on n_{Zr} was used with the exception of polyethylene glycol 20k, where a mass fraction of 20 wt.-%, based on $m_{ZrO(NO_3)_2 \cdot xH_2O}$ was used. The samples were calcined at 973 K.

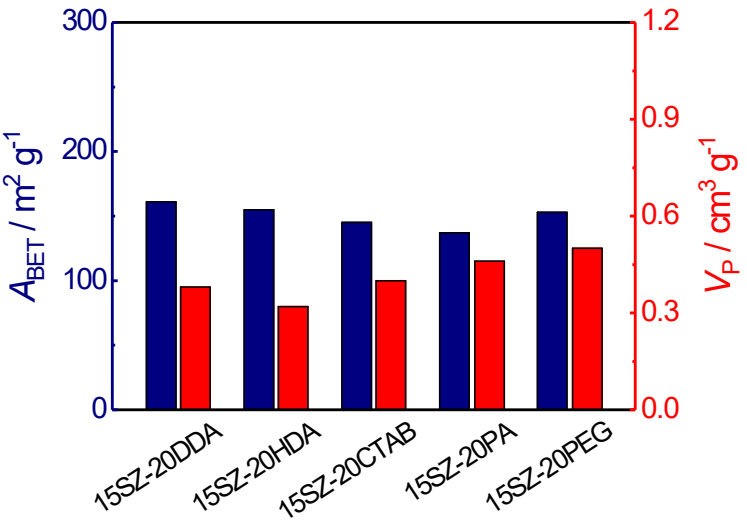

Fig. S28: Specific surface areas and pore volumes of SiO_2-ZrO_2 samples calcined at 973 K prepared using the structure-directing agents dodecylamine (D), hexadecylamine (HD), cetyltrimethyl-ammoniumbromide (CTAB), palmitic acid (PA) and polyethylene glycol 20k (PEG) during gelation.

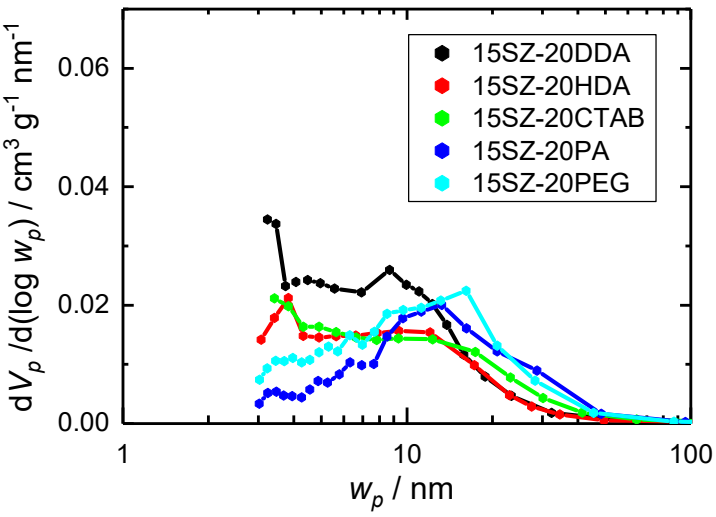

Fig. S29: Pore width distribution of SiO_2-ZrO_2 samples calcined at 973 K prepared using the structure-directing agents DDA, HDA, CTAB, PA and PEG during gelation.

S5 NH_3-Treatment on Zirconia Hydrogels

S5.1 XRD Analysis of Zirconia Samples with and without NH_3-Treatment

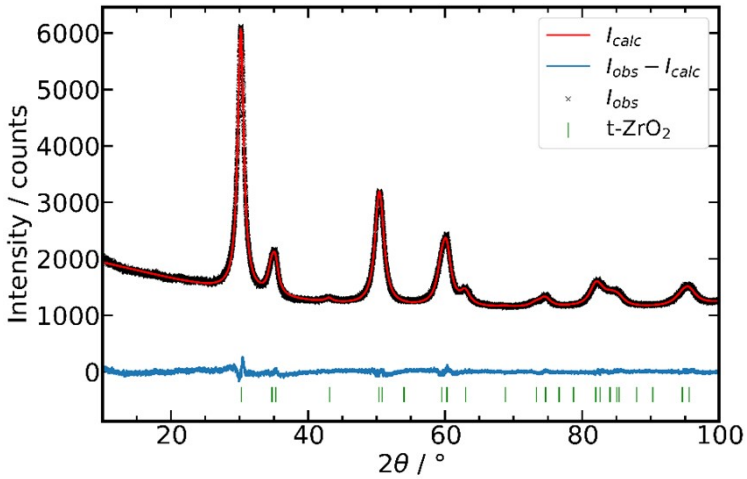

Fig. S30: Rietveld refinement of sample 15SZ-10D, calcined at 923 K; black crosses measured intensity, red line calculated intensity and blue line difference between measured and calculated intensity; green lines Bragg marker tetragonal ZrO_2; R_{exp} = 2.55, R_{wp} = 1.74, R_p = 1.37, GOF = 0.68.

Tab. S14: Structural data obtained from Rietveld refinement of sample 15SZ-10D, calcined at 923 K.

Phase		**ZrO_2 tetragonal**			
Space group		*$P4_2/nmc$* (No. 137)			
Cell Volume in Å^3		66.642(8)			
Cell Mass		246.446			
Crystallite Size *D* in nm		9.12(6)			
Microstrain ε_0		0.00324(3)			
Crystal Density in g/cm^3		6.1408(8)			
Phase Amount in wt.-%		100			
Lattice Parameters					
a in Å		3.59324(17)			
c in Å		5.1615(4)			
Phase		**ZrO_2 tetragonal**			
Atom	*x*	*y*	*z*	B_{iso}	*occ*
Zr1	3/4	1/4	1/4	0.0	1
O1	1/4	1/4	0.4491(3)	0.0	1

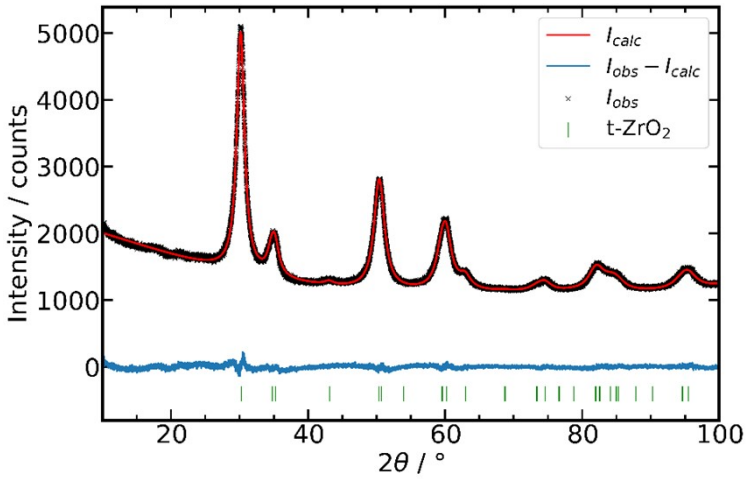

Fig. S31: Rietveld refinement of sample 15SZ-10D-at, calcined at 923 K; black crosses measured intensity, red line calculated intensity and blue line difference between measured and calculated intensity; green lines Bragg marker tetragonal ZrO_2; R_{exp} = 2.56, R_{wp} = 1.62, R_p = 1.28, GOF = 0.63.

Tab. S15: Structural data obtained from Rietveld refinement of sample 15SZ-10D-at, calcined at 923 K.

Phase		**ZrO_2 tetragonal**			
Space group		*$P4_2/nmc$* (No. 137)			
Cell Volume in Å^3		66.720(13)			
Cell Mass		246.446			
Crystallite Size *D* in nm		6.60(4)			
Microstrain ε_0		0.00356(4)			
Crystal Density in g/cm^3		6.1335(12)			
Phase Amount in wt.-%		100			
Lattice Parameters					
a in Å		3.5967(3)			
c in Å		5.1577(7)			
Phase		**ZrO_2 tetragonal**			
Atom	*x*	*y*	*z*	B_{iso}	*occ*
Zr1	3/4	1/4	1/4	0.0	1
O1	1/4	1/4	0.4494(4)	0.0	1

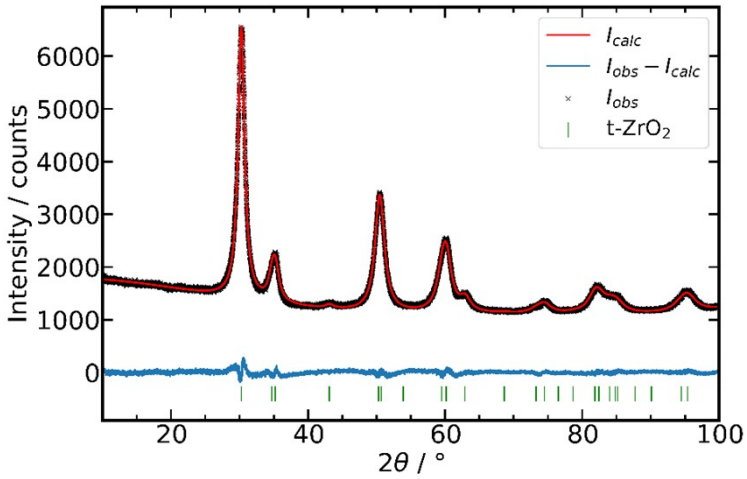

Fig. S32: Rietveld refinement of sample 15SZ-20D, calcined at 923 K; black crosses measured intensity, red line calculated intensity and blue line difference between measured and calculated intensity; green lines Bragg marker tetragonal ZrO_2; R_{exp} = 2.54, R_{wp} = 1.88, R_p = 1.48, GOF = 0.74.

Tab. S16: Structural data obtained from Rietveld refinement of sample 15SZ-20D, calcined at 923 K.

Phase		**ZrO_2 tetragonal**			
Space group		*$P4_2/nmc$* (No. 137)			
Cell Volume in Å^3		66.961(10)			
Cell Mass		246.446			
Crystallite Size *D* in nm		9.88(7)			
Microstrain ε_0		0.00417(3)			
Crystal Density in g/cm^3		6.1116(9)			
Phase Amount in wt.-%		100			
Lattice Parameters					
a in Å		3.60114(19)			
c in Å		5.1634(5)			
Phase		**ZrO_2 tetragonal**			
Atom	*x*	*y*	*z*	B_{iso}	*occ*
Zr1	3/4	1/4	1/4	0.0	1
O1	1/4	1/4	0.4502(3)	0.0	1

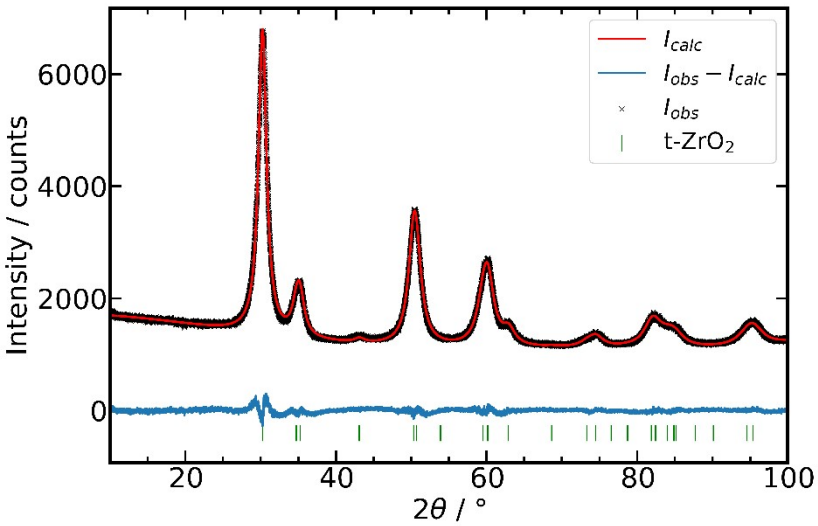

Fig. S33: Rietveld refinement of sample 15SZ-20D-at, calcined at 923 K; black crosses measured intensity, red line calculated intensity and blue line difference between measured and calculated intensity; green lines Bragg marker tetragonal ZrO_2; R_{exp} = 2.51, R_{wp} = 1.97, R_p = 1.52, GOF = 0.79.

Tab. S17: Structural data obtained from Rietveld refinement of sample 15SZ-20D-at, calcined at 923 K.

Phase		**ZrO_2 tetragonal**			
Space group		*$P4_2/nmc$* (No. 137)			
Cell Volume in Å^3		66.915(10)			
Cell Mass		246.446			
Crystallite Size *D* in nm		7.75(4)			
Microstrain ε_0		0.00412(3)			
Crystal Density in g/cm^3		6.1157(9)			
Phase Amount in wt.-%		100			
Lattice Parameters					
a in Å		3.6009(2)			
c in Å		5.1607(5)			
Phase		**ZrO_2 tetragonal**			
Atom	*x*	*y*	*z*	B_{iso}	*occ*
Zr1	3/4	1/4	1/4	0.0	1
O1	1/4	1/4	0.4495(3)	0.0	1

References:

[1] A.A. Coelho, Bruker AXS, J. Appl. Cryst. 51 (2018) 210-218.

[2] H.M. Rietveld, J. Appl. Cryst. 2 (1969).

[3] H.M. Rietveld, Acta Crystallogr. 22 (1967) 151-152.

[4] R.W. Cheary, A. Coelho, J.P. Cline, J. Res. Natl. Inst. Stand. Technol. 109 (2004) 1-25.

[5] R.W. Cheary, A. Coelho, J. Appl. Cryst. 25 (1992) 109-121.

[6] R.L. Snyder, J. Fiala, H.-J. Bunge, Defect and microstructure analysis by diffraction, Reprint, Oxford Univ. Press, Oxford, 2005.

[7] D.K. Smith, W. Newkirk, Acta Crystallogr. 18 (1965) 983-991.

[8] B. Bondars, G. Heidemane, J. Grabis, J. Mater. Sci. 30 (1995) 1621-1625.

[9] J. Schindelin, I. Arganda-Carreras, E. Frise, V. Kaynig, M. Longair, T. Pietzsch, S. Preibisch, C. Rueden, S. Saalfeld, B. Schmid, J.-Y. Tinevez, D.J. White, V. Hartenstein, K. Eliceiri, P. Tomancak, A. Cardona, Nature methods 9 (2012) 676-682.

[10] C. Messaoudii, T. Boudier, C.O. Sanchez Sorzano, S. Marco, BMC bioinformatics 8 (2007) 288.

[11] C.O.S. Sorzano, C. Messaoudi, M. Eibauer, J.R. Bilbao-Castro, R. Hegerl, S. Nickell, S. Marco, J.M. Carazo, BMC bioinformatics 10 (2009) 124.

[12] P. Gilbert, J. Theor. Biol. 36 (1972) 105-107.

[13] K.J. Batenburg, S. Bals, J. Sijbers, C. Kübel, P.A. Midgley, J.C. Hernandez, U. Kaiser, E.R. Encina, E.A. Coronado, G. van Tendeloo, Ultramicroscopy 109 (2009) 730-740.

[14] R.A. Crowther, D.J. de Rosier, F.R.S. Klug, Proc. Roy. Soc. Lond. A 317 (1970) 319-340.